Carbohydrate Polymers 313 (2023) 120870

Contents lists available at ScienceDirect

Carbohydrate Polymers

journal homepage: www.elsevier.com/locate/carbpol

Isothermal titration calorimetry and molecular modeling study of the complex formation of daclatasvir by γ-cyclodextrin and trimethyl-β-cyclodextrin

Paola Peluso [b,*], David Landy [c], Lamia Nakhle [c], Roberto Dallocchio [b], Alessandro Dessì [b], Sulaiman Krait [a], Antonio Salgado [e], Bezhan Chankvetadze [d], Gerhard K.E. Scriba [a,*]

[a] Friedrich Schiller University Jena, Department of Pharmaceutical/Medicinal Chemistry, Philosophenweg 14, 07743 Jena, Germany
[b] Istituto di Chimica Biomolecolare, Consiglio Nazionale delle Ricerche, Traversa La Crucca, 3 - Regione Baldinca - Li Punti, 07100 Sassari, Italy
[c] Université du Littoral-Côte d'Opale (ULCO), Unité de Chimie Environnementale et Interactions sur le Vivant (EA 4492), SFR Condorcet FR CNRS 3417, 145 Avenue Maurice Schumann, 59140 Dunkerque, France
[d] Tbilisi State University, Institute of Physical and Analytical Chemistry, School of Exact and Natural Sciences, 0179 Tbilisi, Georgia
[e] University of Alcalá, NMR Spectroscopy Centre (CERMN), CAI Químicas, Faculty of Pharmacy, 28805 Alcalá de Henares, Madrid, Spain

ARTICLE INFO

Keywords:
Cyclodextrin complexes
Complex stoichiometry
Isothermal titration calorimetry
Molecular dynamics simulation
Daclatasvir

ABSTRACT

The complex formation between daclatasvir and γ-CD or heptakis(2,3,6-tri-*O*-methyl)-β-CD (TM-β-CD) was studied by isothermal titration calorimetry and molecular modeling. Both techniques supported the predominant formation of a 2:1 complex in case of γ-CD although a 1:1 complex may be formed to a much lower extent as well. In case of TM-β-CD the stoichiometry of the complex was exclusively 1:1. Complex formation with γ-CD did not require dissociation of the daclatasvir dimer, which is present in solution, and resulted in a complex with a binding constant of $1.67 \cdot 10^7$ M^{-2}. In contrast, formation of the weak TM-β-CD complex ($K = 371$ M^{-1}) required dissociation of the daclatasvir dimer. This is in line with the observation that the complex formation in case of γ-CD is enthalpy-driven, while the process is entropy-driven in case of TM-β-CD. It is concluded that the plateau observed in capillary electrophoresis is primarily based on the slow dissociation of the daclatasvir-CD complexes caused by steric constrains due to the folded terminal amino acid moieties of daclatasvir exerting a clip effect. In case γ-CD the thermodynamic stability might contribute to the overall slow dissociation.

1. Introduction

Capillary electrophoresis (CE) enantioseparations are based on the formation of transient diastereomeric complexes between the analyte enantiomers and a chiral selector (Chankvetadze, 2018; Fanali & Chankvetadze, 2019), which is added to the background electrolyte (BGE). Among the various compounds applied as chiral selectors in CE, cyclodextrins (CDs) are most often applied (Fejös et al., 2020; Guo & Xiao, 2021; Saz & Marina, 2016; Yu & Quirino, 2019; Zhu & Scriba, 2016) because of several advantages including UV transparency, usability essentially over a large pH range as well as the fact that a large variety of CDs is commercially available.

Daclatasvir (DCV, dimethyl *N*,*N*′-([1,1′-biphenyl]-4,4′-diylbis{1H-imidazole-4,2-diyl-[(2*S*)-pyrrolidine-2,1-diyl][(2*S*)-3-methyl-1-oxobutane-1,2-diyl]})dicarbamate, Fig. 1) is an inhibitor of the hepatitis C nonstructural protein 5A replication complex, which is used in combination with other antiviral drugs for the treatment of infections with hepatitis C virus genotypes 1 to 6 (Pawlotsky et al., 2018). The compound possesses four stereogenic centers resulting in a number of possible stereoisomers. The active drug is the (*S*,*S*,*S*,*S*)-stereoisomer referred to as DCV in the subsequent text. When studying the CD-mediated enantioseparation of DCV and its (*R*,*R*,*R*,*R*)-enantiomer (*RRRR*-DCV) it was noted that an enantioresolution was observed in the presence of some CDs such as randomly methylated β-CD (M-β-CD), while two peaks with a plateau in between were seen in the case of other CDs especially γ-CD (Krait et al., 2020) and *heptakis*(2,3,6-tri-*O*-methyl)-β-CD (TM-β-CD) (Krait et al., 2021). This did not originate from an enantiomerization as the same behavior was observed when either DCV, *RRRR*-DCV or diastereomers such as the *R*,*S*,*S*,*R*-isomer or the *R*,*S*,*S*,*S*-isomer were analyzed in the presence of γ-CD in BGE (Krait et al., 2020).

* Corresponding authors.
E-mail addresses: paola.peluso@cnr.it (P. Peluso), gerhard.scriba@uni-jena.de (G.K.E. Scriba).

https://doi.org/10.1016/j.carbpol.2023.120870
Received 23 October 2022; Received in revised form 17 March 2023; Accepted 27 March 2023
Available online 29 March 2023

Investigation of the structure of the DCV-CD complexes in solution by nuclear magnetic resonance (NMR) techniques revealed two types of complexes between DCV and γ-CD. The minor complex had a ratio of 1:1, while the stoichiometry of the major complex was 2:1 (DCV:γ-CD) (Krait et al., 2020). The formation of an inclusion complex with a guest: host ratio of 2:1 is seldom observed for CDs. In both DCV-γ-CD complexes, the biphenyl moiety of DCV was located inside the CD cavity with the *N*-methoxycarbonyl-valine (MOC-Val) pyrrolidine moieties protruding from the torus. In case of the 2:1 complex, the DCV molecules formed a "stack" with the biphenyl moieties placed on each other (Krait et al., 2020). As stated above, two peaks with a plateau were also observed in the presence of TM-β-CD (Krait et al., 2021). However, for the DCV-TM-β-CD complex 1:1 stoichiometry was concluded from NMR data (Krait et al., 2021). As in case of γ-CD, the biphenyl moiety was included into the cavity and the MOC-Val residues protruded from the torus. Thus, the presence of a plateau in CE experiments was not related to the complex stoichiometry. Interestingly, in case of the CDs yielding an enantioseparation in CE, i.e., β-CD, 2-M-β-CD and 2,6-DM-β-CD, higher order complexes with a stoichiometry of 1:3 (DCV:CD) were deduced from NMR studies (Krait et al., 2021). Again, the biphenyl moiety was located inside the cavity of one CD, while the protruding MOC-Val-pyrrolidine residues were inserted into the cavities of further CD molecules. Based on these studies it could be concluded that the presence of a plateau in CE experiments was not due to an enantiomerization process but due to a slow complexation equilibrium between DCV and γ-CD or TM-β-CD.

The next question was about the cause of the slow association-dissociation equilibrium of the complexes between DCV and these CDs. Therefore, the aim of the present study was the further investigation of the complex formation processes between DCV and γ-CD or TM-β-CD leading to plateau formation observed in CE. The hypothesis was whether this phenomenon in case of the CDs has a unique origin such as unusual high stability of the complexes or if it may be based on different causes. For this purpose, thermodynamic binding data by ITC measurements and molecular modeling were performed.

Molecular modeling has increasingly contributed to the elucidation of CD complex structures by integrating experimental analyses, especially with regard to the binding mechanisms and forces of CD inclusion complexes as well as rationalizing chiral separation mechanisms in liquid-phase enantioseparations (Elbashir, 2012; Elbashir & Aboul-Enein, 2013; Peluso et al., 2019; Peluso & Chankvetadze, 2021). An experimental technique that is also frequently applied to characterization of CD complexes is isothermal titration calorimetry (ITC), which allows direct measurement of enthalpy processes. Based on this, the entropy and enthalpy of the processes as well as the stoichiometry of the complexes and the binding constants (complexation constants, complex formation constants) can be derived (Bertaut & Landy, 2014; Bouchemal & Mazzaferro, 2012; Hansen et al., 2011).

2. Materials and methods

2.1. Chemicals

DCV dihydrochloride was supplied by Mylan Laboratories Ltd. (Hyderabad, India). γ-CD ($C_{48}H_{80}O_{40}$, M_r 1297.2, HPLC purity > 99 %) and TM-β-CD ($C_{63}H_{112}O_{35}$, M_r 1429.6, substitution degree 21, HPLC purity > 97 %) were supplied by CycloLab (Budapest, Hungary). All other chemicals were of analytical grade and obtained from commercial sources.

2.2. Isothermal titration calorimetry

ITC experiments of the CD complexes were performed using a MicroCal iTC_{200} instrument (Malvern Panalytical, Malvern, United Kingdom). DCV and CD solutions were prepared in 0.7 M sodium phosphate buffer, pH 2.5, and subsequently used in the cell (V_0 = 202.8 μL) and the syringe (40 μL), respectively. The concentrations of the analytes used in the respective experiments are outlined in Table S1. These were designed to obtain satisfying accuracy of thermodynamic parameters, by simulating their standard deviation for hypothetical conditions, on the basis of results obtained with preliminary measurements. For experiments using concentrated CD solutions (equal or superior to 5 mM), the CDs were used in both cell and syringe in order to avoid any dilution heat induced by variation of random collision between CD molecules.

In all experiments, after addition of an initial aliquot of 0.5 μL, 10 aliquots of 3.5 μL of the syringe solution were delivered over 7 s for each injection. The time interval between two consecutive injections was defined in order to obtain a systematic and complete return to baseline (100–150 s for TM-β-CD and 1500 s for γ-CD). The agitation speed was 1000 rpm. The resulting heat flow was recorded as a function of time. All measurements were performed at 298.15 K. Prior to data analysis, blank titrations were carried out under the same experimental conditions by injecting buffer into buffer in order to determine the heat induced by injections. These values were subtracted from the measured heats in the presence of DCV and CDs. The peak area following each injection was obtained by integration of the resulting signal and was expressed as the heat effect per injection.

Binding constants (K), inclusion enthalpy (ΔH^0) and entropy contribution (expressed as, $-T\Delta S^0$) and Gibbs free Energy (ΔG^0) were determined using an in-house program developed by Bertaut and Landy (2014), involving an overall analysis of all the binding isotherms obtained for a given CD. One set of thermodynamic parameters was employed for simultaneous nonlinear regression analyses of all

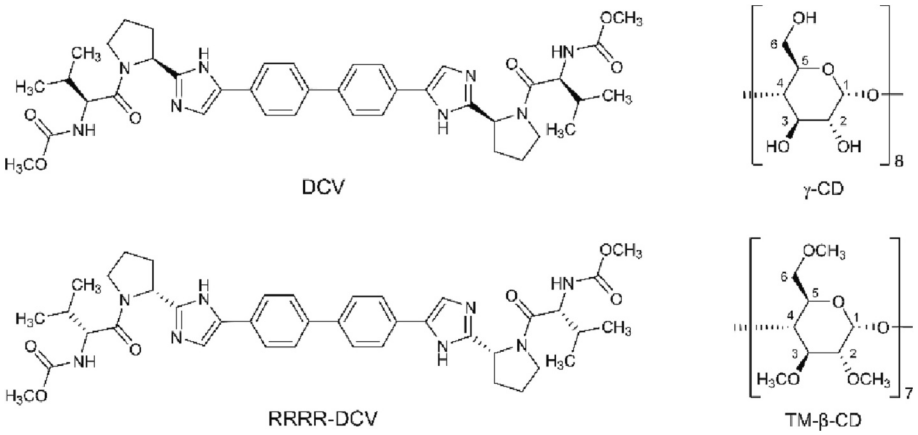

Fig. 1. Structures of daclatasvir, the (*R*,*R*,*R*,*R*)-enantiomer, γ-CD and TM-β-CD.

experiments for a given DCV/CD system. Models involving mixtures of complexes (from 1:1 to 1:3 and from 1:1 to 3:1 inclusion compounds) were evaluated on the basis of dedicated binding polynomials. The results are reported for the model leading to the best agreement between experimental and theoretical heats.

2.3. Capillary electrophoresis

CE experiments were performed as described by Krait et al. (2020) using a Beckman P/ACE MDQ capillary electrophoresis system (Beckman Coulter, Krefeld, Germany) equipped with a UV–Vis diode array detector set at 305 nm. Analysis was carried out in a 40/50.2 cm, 50 μm i.d., 365 μm o.d. fused-silica capillary from CM Scientific (Silsden, UK) using 50 mM sodium phosphate buffer containing the appropriate amount of γ-CD as BGE at a capillary temperature of 25 °C and an applied voltage of 25 kV. Integration of the electropherograms and simulations were realized using a dedicated homemade Octave script.

2.4. Molecular modeling

The 3D structures of γ-CD and TM-β-CD were released from Cambridge Structural Database (CSD) (Thomas et al., 2010), entries MUXBIT (Catenacci et al., 2020) and GELKEN10 (Harata et al., 1992), respectively. All structures were prepared using the build function and model kits and tools provided by Spartan'10 Version 1.1.0 (Wavefunction Inc., Irvine, CA, USA) program (Shao et al., 2006) for building and editing organic molecules. The 3D structures of DCV, *RRRR*-DCV *RSSR*-DCV, the isoleucine analog Ile-DCV, the analog lacking a MOC-Val side chain (Mono-DCV) as well as the synthetic precursors BOC-bis-pyrrolidinyl-imidazolyl biphenyl (BOC-BPIB) and bis-pyrrolidinyl-imidazolyl biphenyl (BPIB) (for the structures of DCV stereoisomers and analogs see Fig. S1, Supplementary material), were treated as fully protonated in accord with the experimental pH = 2.5.

2.4.1. Electrostatic potential analysis of DCV and its analogs

Computation of lowest energy conformations and electrostatic potential isosurfaces (V_S) (isovalue 0.002 au) (given in kJ·mol^{-1}) of DCV and its analogs were performed employing the Hartree-Fock (HF) method with 3-21G* as basis set and at density functional theory (DFT) level (B3LYP/6-311G*). The electrostatic potential in a point r (V(r)) is given by Eq. (1):

$$V(\mathrm{r}) = \sum_{\mathrm{A}} \frac{Z_{\mathrm{A}}}{R_{\mathrm{A}} - \mathrm{r}} - \int \frac{\rho(\mathrm{r})d\mathrm{r}'}{|\mathrm{r}' - \mathrm{r}|} \quad (1)$$

where Z_A is the charge on nucleus A located at R_A, and ρ(r) is the electron density function. The sign of V(r) is positive or negative if the effect of the nuclei (first positive term) or that of electrons (second negative term) is dominant, respectively. The V_S maps were graphically generated through the graphical interface of Spartan'10 and, by convention, colors toward red depict negative potential, while colors toward blue depict positive potential, and colors in between (orange, yellow, green) depict intermediate values of potential.

2.4.2. Construction of CD-complexes and MD simulations

The complexes between DCV and *RRRR*-DCV and the two CDs were modeled by manually docking each analyte into the CD cavity. Then, each complex was submitted to a conformational systematic search using the Monte-Carlo algorithm, examining 1000 conformers spanning possible shapes open to a flexible molecule without consideration of energy, and keeping 10 low-energy conformers. On this basis, the lowest-energy conformations of all complexes underwent geometry optimization using the MMFF94s force field.

For MD simulations, geometry optimization of all molecules and point charge derivation were achieved by means of the AM1-BCC method (Jakalian et al., 2000), as implemented in the *sqm* program (Walker et al., 2008) contained in the AMBER Tools (Case et al., 2005) distribution. The Generalized Amber Force Field (GAFF) and the GLYCAM04 (Basma et al., 2001; Kirschner & Woods, 2001a,b) parameter sets (Case et al., 2018) were used for all atoms. Chimera 1.13.1 (Pettersen et al., 2004) was also employed for visualization of MD trajectories and 3D figure generation. The complexes between the analyte enantiomers and the CDs were modeled as obtained from the MMFF94 geometry optimization. Each complex was then immersed in a box of TIP3P water molecules that extended 20 Å away from any solute atom. In order to achieve electroneutrality in the simulated systems, the positive charge of DCV and derivatives in the CD complexes was neutralized by substituting one chloride ion for a water molecule located close to the most positive electrostatic potential region. Running the AMBER *pmemd.cuda* (Salomon-Ferrer et al., 2013) code in parallel on 4 GeForce Nvidia RTX2080 Ti graphics processing units (GPUs), each simulation contained the following stages. Periodic boundary conditions were applied to simulate a continuous system. Upon reorientation of all solute hydrogens and water molecules, first, a 1000-steps solvent minimization was performed using the steepest descent method with macrocycle restrained via a force of 40 kcal·mol^{-1}. Then, the system was gradually heated over 0.5 ns to a target temperature with the macrocycle restrained via a force of 40 kcal·mol^{-1}. The solvent underwent a 1000-steps minimization with a restriction of 40 kcal·mol^{-1}. A short 0.2 ns NPT ensemble MD run was performed with a 30 kcal·mol^{-1} restrain, followed by another 10,000-steps energy minimization process. Then, another 0.1 NPT ensemble MD run was performed with a force of 20 kcal·mol^{-1}, followed by a 10,000-steps minimization with restrictions of 20 kcal·mol^{-1}. A re-heating over 60 ps of the system at a constant volume to the target temperature was performed with a restriction of 20 kcal·mol^{-1}. A 20,000-step minimization was performed with restrictions of 20 kcal·mol^{-1}. NPT ensemble 2 ns MD was performed, restriction gradually decreasing from 20 kcal·mol^{-1} to the unrestricted system. The Langevin thermostat was used to maintain the simulation temperature. Finally, the production step was carried out under the equilibrium conditions, and the system was subjected to 100 ns MD simulation for each complex, if not indicated otherwise. 100 ns of the trajectories from each case were considered for statistical analysis. The application of SHAKE to all bonds allowed an integration time step of 2 fs to be used. A cut-off distance of 8 Å was used for the nonbonded interactions and the list of nonbonded pairs was updated every 25 steps. Periodic boundary conditions were applied, and electrostatic interactions were represented using the smooth particle mesh Ewald method (Darden et al., 1993) with a grid spacing of 1 Å. The coupling constant for the temperature and pressure baths was 0.2 ps. The resulting set of 2500 structures for each complex was analyzed with the *cpptraj* module in AMBER (Roe & Cheatham, 2013) to measure relevant distances and angles, along with R scripts (Core Team, 2017) developed in house.

For each complex, the total interaction energy was calculated. The reported energies are mean values that were calculated from 2500 × 3 complexes extracted by snapshots taken every 40 ps from the trajectories of three 100 ns MD replicates, if not indicated otherwise. The interaction energy (E_{int}) between the analyte enantiomer and CD was calculated on the basis of the energies of the enantiomer-CD complex, CD, and the analyte enantiomer (Eq. (2)):

$$E_{\mathrm{int}} = E_{\mathrm{enantiomer-CD\ complex}} - E_{\mathrm{enantiomer(s)}} - E_{\mathrm{CD}} \quad (2)$$

where the E_{int} term is derived from the contributions of the van der Waals (vdW) (E_{vdW}) and the electrostatic interaction (E_{el}) energy terms (Eq. (4)):

$$E_{\mathrm{int}} = E_{\mathrm{el}} + E_{\mathrm{vdW}} \quad (3)$$

2.4.3. Calculation of the binding energy difference for the TM-β-CD complexes

For the complexes DCV-TM-β-CD and *RRRR*-DCV-TM-β-CD, the geometry optimization procedures were performed in vacuum and water

(SM5.4 model) (Chambers et al., 1996). The binding energy ($E_{binding}$) (kcal·mol^{-1}) between the enantiomers and the TM-β-CD was determined on the basis of the calculated energies (MMFF94 and PM6 semi-empirical) of the CD/enantiomer complex, CD and enantiomer (Eq. (4)):

$$E_{binding} = E_{complex} - E_{enantiomer} - E_{CD} \quad (4)$$

3. Results and discussion

3.1. Isothermal titration calorimetry

ITC was employed for the determination of the binding constants, the enthalpy and entropy as well as the Gibbs free energy of the formation of the complexes of DCV with γ-CD or TM-β-CD. When a 5 mM buffered solution of DCV was injected into the cell containing CD-free buffer, significant positive peaks were obtained (Fig. S2A, Supplementary material). Changes of the integrated heats (Fig. S2B, Supplementary material) are in agreement with the dissociation of a pre-formed dimeric DCV_2 associate. The formation constant of the dimer is weak (K around 175 M^{-1}) and its dissociation is exothermic (ΔH^0 around −9600 cal·mol^{-1}) as well as entropy-driven. In the presence of a CD in the cell or in both cell and syringe, the monomer-dimer equilibrium of DCV is disturbed so that the respective calorimetric traces strongly differ depending not only on the CD concentration but also on the stoichiometry and thermodynamics of the DCV-CD complexes (Figs. S3 and S4, Supplementary material). The experimentally determined heats were fitted to the best model considering all possible DCV-complexes with different stoichiometries. The respective thermodynamic data are compiled in Table 1. All processes proved to the exothermic characterized by a negative enthalpy of inclusion as generally observed for CD complexes (Rekharsky & Inoue, 1998).

In the case of TM-β-CD, only a 1:1 complex was found, which is in agreement with NMR and mass spectrometry data (Krait et al., 2021) as well as molecular modeling (see below). As indicated by the complexation constant, the complex is only about twice as stable as the DCV dimer. In the case of DCV/TM-β-CD complexation, the stoichiometry of the complex is 1:1. Since DCV is partially present in the solution as a dimer, its complexation with TM-β-CD can be represented as a sum of following two consecutive coupled equilibria: (1) dissociation of the DCV dimer and (2) complexation of the resulting DCV monomer by TM-β-CD. Entropy changes of the overall process were positive as indicated by the negative value of $-T\Delta S^0$, i.e., in this case complex formation is entropy-driven. Thus, the first process proceeds with an entropy gain that is significantly larger than the entropy loss of the second process resulting in an overall positive algebraic sign for the entropy of the two-stage coupled process.

In the case of γ-CD, the preferential formation of a 2:1 complex was derived, confirming NMR and mass spectrometry studies (Krait et al., 2020) as well as molecular modeling data (see below). The complex proved to be very stable with a binding constant of $1.67 \cdot 10^7$ M^{-2}. This high stability can explain the phenomenon observed in CE, i.e., the persistence of the complex during analysis with a CD-free BGE upon injection of a sample containing DCV and γ-CD (Krait et al., 2020). The simultaneous presence of a 1:1 complex as concluded from NMR and mass spectrometry (Krait et al., 2020) could not be confirmed by ITC but can also not be excluded because none of the experiments allowed to distinguish between a 2:1 binding model and a "1:1 plus 2:1 model". A possible reason for this could be the fact that the 1:1 complex is significantly weaker by several orders of magnitude compared to the 2:1 complex so that it is not detected under the experimental ITC conditions. Thus, in order to assess the existence of the 1:1 DCV-γ-CD complex and to estimate the corresponding formation constant, ITC results were combined with CE data (Fig. S5, Supplementary material). Considering that the 2:1 DCV_2-γ-CD complex was in slow exchange with DCV, DCV_2 and DCV-γ-CD, CE peak areas were used to evaluate the percentage of DCV in the 2:1 complex dividing the first peak attributed to the 2:1 complex by the area of both peaks for total γ-CD concentration. Percentages were simulated by resolving the binding polynomials resulting from the equilibria between DCV, DCV_2, DCV-γ-CD and DCV_2-γ-CD, which were also used in ITC data treatment, for each total concentrations of γ-CD, $[\gamma CD]_T$, and DCV, $[DCV]_T$. These can be defined on the basis of the concentrations of free γ-CD, $[\gamma CD]$, and free DCV, $[DCV]$, the DCV dimerization constant, K_{DCV2}, and the constants of the 1:1 and 2:1 complexes, $K_{1:1}$and $K_{2:1}$, respectively, defining a cumulative formation constant for the 2:1 complex, $\beta_{2:1} = K_{1:1} \cdot K_{2:1}$, according to Eqs. (5) and (6):

$$[\gamma CD]_T = [\gamma CD] + (K_{1:1} \cdot [\gamma CD] \cdot [DCV]) + (\beta_{2:1} \cdot [\gamma CD] \cdot [DCV]^2) \quad (5)$$

$$[DCV]_T = [DCV] + (2 \cdot K_{DCV2} \cdot [DCV]^2) + (K_{1:1} \cdot [\gamma CD] \cdot [DCV]) + (2 \cdot \beta_{2:1} \cdot [\gamma CD] \cdot [DCV]^2) \quad (6)$$

Considering fixed values for $\beta_{2:1}$ and K_{DCV2} (determined by ITC) and resolving such systems with two equations and two unknown parameters ($[\gamma CD]$ and $[DCV]$) allowed to simulate the concentration of each species. Subsequently, theoretical percentages were fitted to the percentages derived from CE by varying the $K_{1:1}$ value (Fig. S5B, Supplementary material). Accordingly, the fit obtained for the minimal root mean square deviation between data was used to extract $K_{1:1}$ which resulted in a value for $K_{1:1}$ of 71 ± 6 M^{-1}.

Furthermore, the kinetics of the interaction between DCV and γ-CD was extremely slow on the ITC timescale. Typically, interactions between CDs and analytes are fast as observed for β-CD and the methylated derivatives. Thus, peaks lasting up to 1 min were observed for TM-β-CD in the thermograms (Fig. S3, Supplementary material), while peaks lasting about 10 min were seen for γ-CD (Fig. S4, Supplementary material). This could result from the requirement of a specific arrangement of the dimeric DCV associate to fit into the CD cavity or a conformational adjustment of the CD ring upon inclusion of the dimeric DCV.

Complex formation in case of γ-CD is enthalpy driven as indicated by the positive $-T\Delta S^0$ value (Table 1). This may be explained by the fact that dissociation of the DCV dimer is not required because the dimer might be directly accommodated in the CD cavity. Moreover, as shown by the molecular modeling below, this might result from the tight fit of the dimer in the γ-CD cavity leading to poor freedom between host and guest. The value of the Gibbs free energy, ΔG^0, is about threefold higher in case of γ-CD as compared to TM-β-CD (Table 1).

Thus, steric constrains seem to be the major reason for the plateau phenomenon observed in CE in the presence of γ-CD as well as TM-β-CD. In case of γ-CD as host, an additional thermodynamic contribution

Table 1
Complexation constants, K, enthalpy, ΔH^0, entropy expressed as $-T\Delta S^0$ and Gibbs free energy, ΔG^0, of the complex formation between DCV as well as of DCV-CD systems. The numbers in brackets refer to SD values.

	K (M^{-1})	ΔH^0 (cal·mol^{-1})	$-T\Delta S^0$ (cal·mol^{-1})	ΔG^0 (cal·mol^{-1})
DCV_2[a]	194 (11)	−9380 (112)	6262 (146)	−3118 (34)
DCV–TM-β-CD (1:1)	371 (17)	−536 (130)	−2965 (157)	−3501 (27)
DCV_2[a]	163 (8)	−9703 (86)	6688 (115)	−3015 (29)
DCV_2–γ-CD (2:1)	$1.67 \cdot 10^7$ ($3 \cdot 10^5$)	−14,615 (79)	4772 (90)	−9843 (11)

[a] Experiment in the absence of the CD performed before each series of experiments.

(formation of a highly stable complex) might be considered, while this is not the case for TM-β-CD.

3.2. Molecular modeling

The associates under investigation were modeled using

(a) MD simulations in order to assess the dynamic features of the DCV-CD complexes and the main noncovalent interactions underlying the complex,
(b) electrostatic potential analysis to quantify the contribution of the molecular properties of DCV to the observed phenomena, and
(c) MMFF94s and PM6 semiempirical in vacuum and in water comparatively, in order to evaluate the impact of neglecting the solvent to calculate binding free energy of the complexes and related differences.

The virtual structures of γ-CD and TM-β-CD were modeled and characterized as reported in the Supplementary material (γ-CD: Figs. S6 to S9; TM-β-CD: Figs. S13 and S14). The geometrical parameters of the non-complexed macrocycles were considered as reference for comparison with the DCV complexes in order to evaluate the degree of possible distortions occurring in the CD structure after analyte-CD complex formation. A suitable compromise between computational time and the need to obtain a virtual model as reliable as possible to describe and explain the observed phenomena was the criterion guiding the choice of methods, basis sets, and parameter sets used for modeling the CDs, the analytes and their related complexes.

3.2.1. Complexes of DCV with γ-CD

The dynamic behavior of the 1:1 and 2:1 DCV-γ-CD and *RRRR*-DCV-γ-CD complexes was explored in MD simulations performed over 100 ns in the AMBER force field by treating the solvent water explicitly. The mean interaction energy of each complex was extracted from the MD trajectories. As shown in Fig. 2 for both the 1:1 (Fig. 2A and B) and 2:1 (Fig. 2C and D) complexes, the DCV complexes showed similar interaction energies compared to the *RRRR*-DCV complexes. The 2:1 complexes showed higher thermodynamic stability compared to the 1:1 complexes. The contribution of E_{el} to the total interaction energy was similar to the contribution of the E_{vdW} term in case of the 1:1 complexes, whereas it was higher in the case of the 2:1 complexes (Table 2). In accordance, the overall hydrogen bonding (HB) lifetime (Table S2, Supplementary material) between DCV and γ-CD was lower for the 1:1 complex (37 ns) compared to the 2:1 complex (109 ns). However, the contribution of the E_{vdW} was relevant in both cases, confirming that the contacts between the central biphenyl moiety of DCV and the

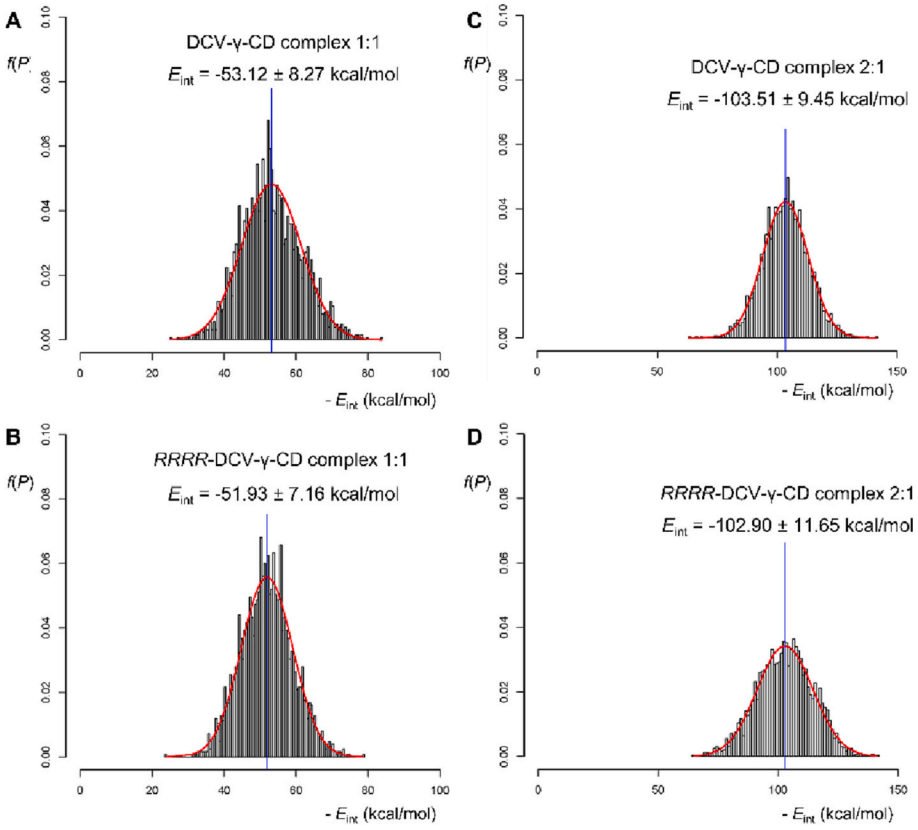

Fig. 2. Distribution of interaction energies of DCV-γ-CD (A, C) and *RRRR*-DCV-γ-CD (B, D) complexes over 3 cycles of 100 ns MDs (2500 frames/simulation).

Table 2
Mean interaction energies of the DCV-γ-CD and *RRRR*-DCV-γ-CD complexes extracted by MD trajectories.

Complex	$E_{interaction}$ (kcal·mol^{-1})	E_{el} (kcal·mol^{-1})	E_{vdW} (kcal·mol^{-1})
DCV-γ-CD (1:1)	−53.12 ± 8.27	−27.40 ± 7.51	−25.72 ± 3.19
RRRR-DCV-γ-CD (1:1)	−51.93 ± 7.16	−25.46 ± 5.95	−26.47 ± 3.19
DCV-γ-CD (2:1)	−103.51 ± 9.45	−61.45 ± 9.02	−42.06 ± 2.66
RRRR-DCV-γ-CD (2:1)	−102.90 ± 11.65	−55.85 ± 10.92	−47.05 ± 3.83

hydrophobic inner cavity of γ-CD were important components of the analyte-macrocyle interaction.

Using the GLYCAM04 force field in place of GAFF with the 2:1 DCV-γ-CD complexes provided very similar results in terms of interaction energies (DCV-γ-CD, 102.13 ± 14.02 kcal/mol; *RRRR*-DCV-γ-CD, 103.99 ± 18.35 kcal/mol).

It has been demonstrated that the liberation of high-energy water from the cavity of CDs is a pivotal driving-force for CD-complex formation (Sandilya et al., 2020). Thus, the average number of water molecules inside the γ-CD cavity was calculated before and after the formation of the complexes, obtaining a $\Delta n_{H2O} = 5 \pm 3$ and $\Delta n_{H2O} = 8 \pm 3$ for the 1:1 and 2:1 DCV-γ-CD complexes, respectively. Thus, the liberation of high-energy water from the cavity of the γ-CD could function as a stabilizing factor, which is more prominent for the 2:1 complex than for the 1:1 complex.

Despite the fact that the DCV enantiomers remained always in the complexed form during the 100 ns of the MD simulations, a higher mobility of DCV and *RRRR*-DCV inside the γ-CD cavity along its axis was observed as illustrated in Fig. 3. Positions A and C represent folded structures at one of the two terminal MOC-Val residues, while the most stable form B contains folded residues at both ends of the molecules. A much lower mobility of DCV inside the cavity was observed in the case of the 2:1 complexes. Fig. 4 shows a representative snapshot of the 2:1 DCV-γ-CD complex. In Table S3 (Supplementary material), the main noncovalent interactions featuring this structure are summarized. Overall, five HBs appear to stabilize the DCV-γ-CD complex as well as the conformation of DCV at the wider CD rim. Three intermolecular HBs between DCV molecules and γ-CD with a lifetimes of 81, 24 and 2 ns, two of which also stabilize the folded conformation (HBs A and E in Table S3). Two HBs with lifetimes of 82 and 18 ns, respectively, ensure the folded conformation as well as stabilization of the dimer. With regard to the narrower rim, inter- and intramolecular HBs involving the DCV molecules could be observed as the main interactions stabilizing folded conformation with lifetimes ranging from 2 to 13 ns, and two negligible DCV-CD HBs involving the primary hydroxyl group with lifetimes of 0.04 and 0.08 ns, respectively (data not shown).

The different dynamics as a function of the stoichiometry of the complexes may also explain the different stability of the 1:1 complex compared to the 2:1 complex. Indeed, during the motion between the forms A ↔ B ↔ C in the 1:1 complex (Fig. 3) the terminal residues moved from the folded to the unfolded form, the latter structure would favour a dissociation, due to the reduced steric constraint. In contrast, the terminal MOC-Val moieties remained in the folded conformation in the 2:1 complex over 100 ns of MD simulations (Fig. 4), likely due to the steric hindrance generated by the confinement of two DCV molecules in the CD cavity. The folded conformation of DCV and its enantiomer exerted a "clip-effect" on the CD rims contributing to slow complex dissociation.

Further information resulted from the analysis of the MD trajectory of the 2:1 Mono-DCV-γ-CD complex. Mono-DCV lacks one MOC-Val moiety compared to DCV (Fig. S1, Supplementary material) and only a single peak (and no plateau) was observed in CE analysis. Moreover, NMR analysis also hinted at the formation of a 2:1 Mono-DCV-γ-CD

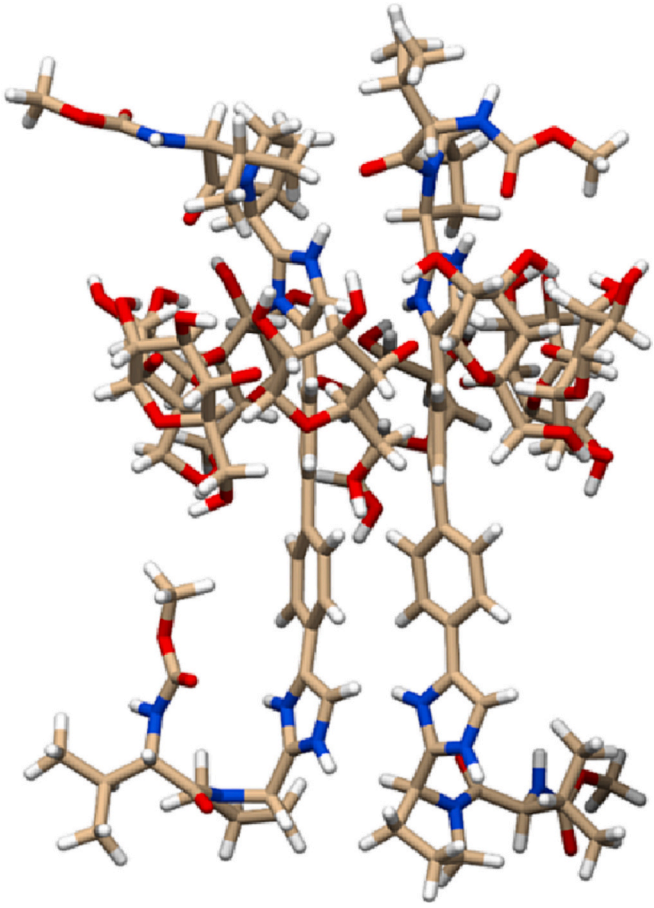

Fig. 4. Representative snapshot of the most frequent 2:1 DCV-γ-CD complexes observed over 100 ns of MD simulations.

complex (Krait et al., 2020), for which an interaction energy of 104.51 ± 11.97 kcal·mol^{-1} (E_{el} = 59.49 ± 10.86 kcal·mol^{-1}; E_{vdW} = 45.02 ± 2.99 kcal·mol^{-1}) was extracted from the MD trajectories, which is very close to the values of the 2:1 DCV-γ-CD complex (Table 2). This would confirm that a 2:1 complex was also formed in the case of Mono-DCV as hypothesized from NMR analysis (Krait et al., 2020). Moreover, the similarity of the interaction energies of the γ-CD complexes of DCV and Mono-DCV confirmed the importance of the biphenyl moiety as interaction site with the CD cavity, given that the interaction energy was not affected by the absence of one terminal MOC-Val residue. However, the lack of one terminal residue could favour a faster complex dissociation of the Mono-DCV-γ-CD 2:1 complex compared to the DCV-γ-CD 2:1 complex, so that a plateau was not observed in CE when analyzing Mono-DCV. Considering the steric constraints due to the folded MOC-VAL side chains discussed above, a slow dissociation of the 2:1

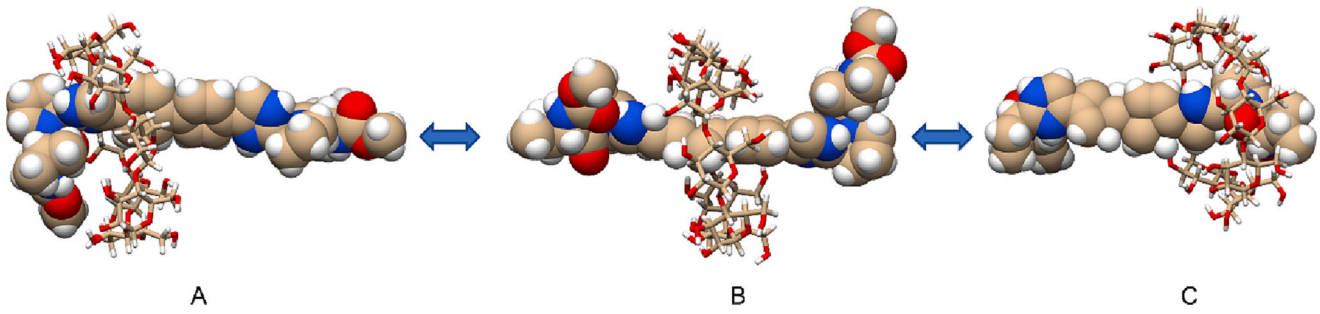

Fig. 3. Motion between three representative forms A – B – C observed for the 1:1 DCV-γ-CD complexes over 100 ns of MD simulations.

complex can be assumed.

As shown in Fig. S10 (Supplementary material), a slight deformation of the symmetric shape of the γ-CD macrocyle was found over 100 ns of MD simulations in case of the 1:1 DCV-γ-CD complex (Fig. S10A and B) and the 2:1 DCV-γ-CD complex (Fig. S10C and D) compared to non-complexed γ-CD (Fig. S8). As an effect of this deformation, the CD would further block the guest inside the cavity. Thus, deformation of the inner cavity of the γ-CD to a slightly elliptic form in the complexed state might be considered as a second "steric effect" contributing to slow the dissociation of the 2:1 DCV-γ-CD complex. The effect could likely be due to a conformational adjustment of the host structure after the complexation in order to stabilize the system. However, despite this slight distortion, the most frequent conformation of the glucosyl units remained the $^4C_1$ chair conformation in all γ-CD complexes (≥87 ns over 100 ns in case of the complex versus ≥95 ns over 100 ns for free γ-CD).

With the aim to explore the complexation process and the non-covalent interactions driving the inclusion of DCV dimer in the γ-CD, the dimer was docked outside the CD cavity and the contacts between analyte dimer and γ-CD were evaluated over 100 ns MD using GLYCAM04 as force field. A complete inclusion of the DCV dimer was not observed even increasing the simulation time to 4 microseconds. However, an interesting picture of the inclusion of the DCV tails into the γ-CD was obtained (Table 3), observing that both DCV-DCV and DCV-CD intermolecular HBs orientated the DCV dimer to enter into the macrocycle cavity.

Moreover, the dynamics of DCV dimer formation over 160 ns MD was modeled (Fig. 5) showing that the dimer formed through a first tail-to-tail contact driven by intermolecular HBs. The dimer proved to be very stable over 160 ns (4000 frames), with the distance between the biphenyl system remaining below 6 Å for 120 ns (2999 frames) (Fig. S11, Supplementary material).

On the basis of the ITC and MD results, the formation of the DCV dimer in solution may favour the formation of the 2:1 DCV-γ-CD complex, which seemed to determine plateau-shaped electropherograms in CE (Krait et al., 2020). Moreover, a plateau was also observed for the *RSSR*-DCV diastereomer as well as the isoleucine analog Ile-DCV, while only a single peak resulted in case of Mono-DCV as well as BOC-BPIB and BPIB (for structures see Fig. S1, Supplementary material) (Krait et al., 2020). In an attempt to understand the molecular cause for the formation of complexes with 2:1 stoichiometry and the slow complexation equilibrium resulting in plateau-shaped electropherograms in CE, the electron charge density of DCV and some derivatives in terms of V_S (0.002 au) (Spartan '10, HF/3-21G* and DFT/B3LYP/6-311G*, vacuum) and isosurface area and volume were calculated (Fig. S12). The V_S minima ($V_{S,min}$) were associated with higher electron charge density of the inspected molecular regions, whereas V_S maxima ($V_{S,max}$) revealed lower electron charge density regions.

Comparing the size of the compounds and their V_S extrema ($V_{S,min}$ and $V_{S,max}$) (Fig. 6 and Table S4, Supplementary material), the following conclusions can be drawn:

Table 3
Intermolecular hydrogen bonds (HBs) (distances) driving the inclusion of the DCV dimer into the γ-CD complex (wider CD rim) observed through MD simulation.

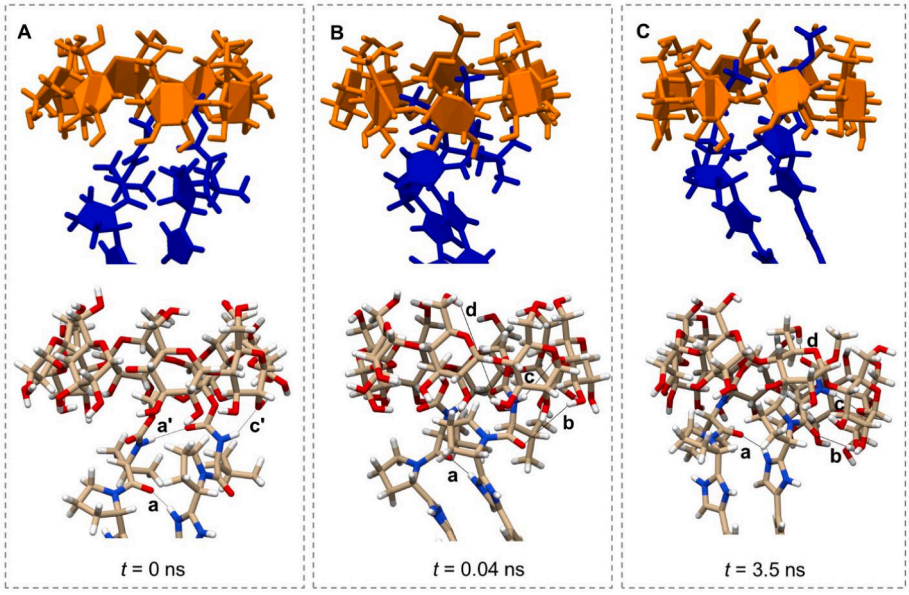

				Length (Å)		
HB	Type	Acceptor	Donor	0 ns	0.04 ns	3.5 ns
a	DCV_1-DCV_2	C=O	N-H	1.718	1.807	1.805
a'	DCV_1-DCV_2	N-H	C=O	2.299	--	--
b	DCV_2-CD	C=O	O(3)H	--	3.850	2.253
c	DCV_2-CD	N-H	$O_{glycosidic}$	--	3.048	2.238
c'	DCV_2-CD	N-H	O(2)H	2.573	--	--
d	DCV_2-CD	C=O	O(6)H	--	7.433	1.550

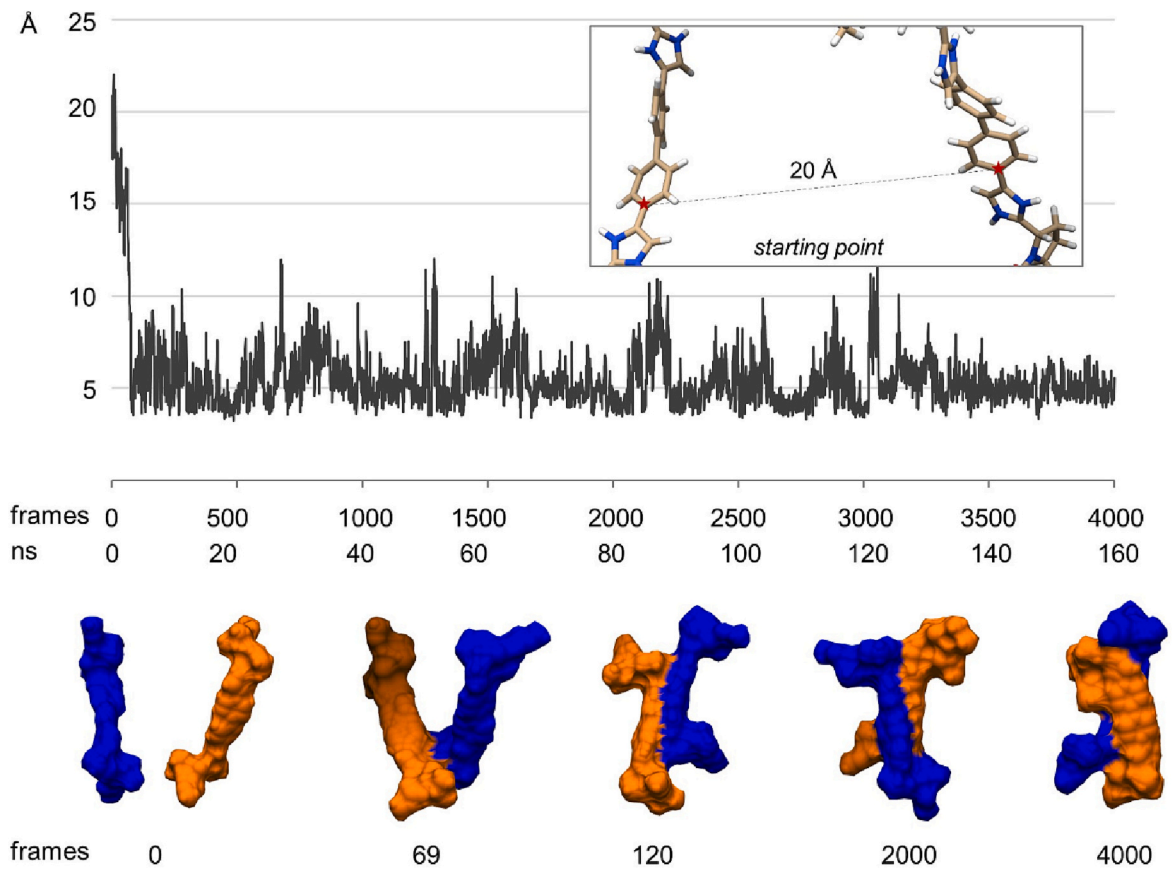

Fig. 5. DCV-DCV dimer formation and distribution of the distances between the two aromatic carbons of two interacting DCV molecules (highlighted with the red stars in the insert) over 160 ns MD (4000 frames), initial distance = 20 Å. (For interpretation of the references to color in this figure legend, the reader is referred to the web version of this article.)

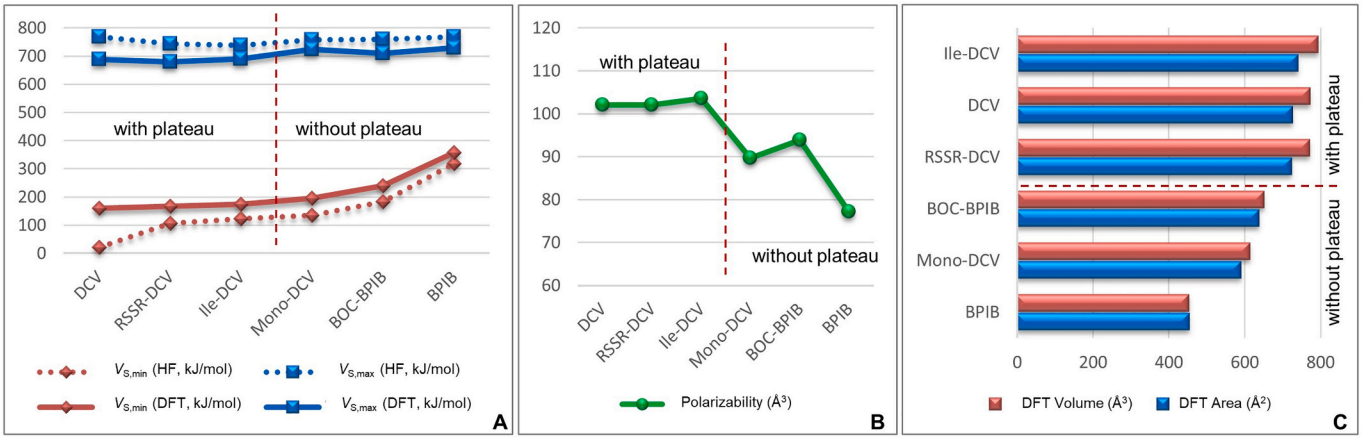

Fig. 6. Stereoelectronic properties of DCV, *RSSR*-DCV, Ile-DCV, BOC-BPIB, Mono-DCV and BPIB. (A) V_S ranges, (B) polarizability, and (C) area and volume values of the electron density isosurfaces.

(1) As shown in the course of the MD simulations of DCV-γ-CD complexation, all compounds providing a plateau-shaped electropherogram, i.e., DCV, *RSSR*-DCV and Ile-DCV, showed a common shape with a folded structure at both terminal MOC-Val moieties. This feature was present to a lesser degree in the case of BOC-BPIB, whereas it was absent in Mono-DCV (at one terminus) and BPIB. The folded structure of the terminal amino acid residues could favour a slow complex dissociation process due to a clip-effect exerted by the terminal side chains toward the CD rims.

(2) For compounds, which did not display plateau-shaped electropherograms, the area and volume values of the calculated electron density isosurfaces (Fig. 6C), as well as polarizability decreased (Fig. 6B). Moreover, the overall electron charge density decreased for these compounds as well. The lowest $V_{S,min}$ value was found for DCV (HF, 20.6 kJ·mol^{-1}; DFT,159.82 kJ/mol) and it increased to 318.4 kJ·mol^{-1} (HF) and 357.79 kJ·mol^{-1} (DFT) in the case of BPIB (Fig. 6A).

(3) The biphenyl system was more π-acidic in compounds that do not provide plateau-shaped electropherograms compared to

compounds showing this feature. Thus, a higher electron charge density seems to determine the higher capability of the analyte to form dimeric associates in the CD cavity, i.e., 2:1 analyte-γ-CD complexes.

(4) Accordingly, the electron charge density on the carbonyl groups bonded to the pyrrolidine ring (N_{pyr}-C=O) was lower (higher V_S) for BOC-BPIB and Mono-DCV (HF: $V_{S,min}$ = 183 and 135 kJ·mol^{-1}, respectively), which do not display the plateau phenomenon in CE with γ-CD compared to DCV, RSSR-DCV or Ile-DCV (HF: $V_{S,min}$ = 97, 106, and 122 kJ·mol^{-1}, respectively) showing the plateau-effect in CE.

Thus, V_S analysis confirmed that, along with the properties of the macrocycle host, the stereoelectronic features of the analyte impact the complexation equilibrium, which is slower when the analytes (a) feature folded terminal amino acid-derived moieties and more extended areas and volumes of the related electron density isosurfaces (*steric effect*) (Fig. 6C), and (b) a higher electron charge density (lower $V_{S,\ min}$) on the main interaction sites, which are the central biphenyl system and the polar terminal groups (*electronic effect*) (Fig. 6A and B).

In conclusion, the calculations by MD simulations and *V* analysis demonstrated that five factors could impact complexation of DCV as well as stereoisomers and related derivatives by γ-CD resulting in the formation of a strong complex as indicated by the high complexation constant found by ITC:

(1) an electronic effect related to the electron charge density distribution of the analytes,
(2) a steric effect depending on the spatial dimensions of the analytes,
(3) a steric effect due to the folded conformation of the terminal MOC-amino acid residues, which act as a clip toward the CD rims,
(4) a steric effect generated by the slight elliptic distortion of the γ-CD ring upon complexation of DCV and analogs acting as a clamp toward the analyte,
(5) in terms of interactions, HBs could contribute to complex formation and stabilization (HB lifetime was lower for the 1:1 complex compared to the 2:1 complex). Intermolecular HBs also showed to drive and underlie the formation of the DCV dimer. In addition, the hydrophobic contacts between the biphenyl moiety and the inner cavity of γ-CD appeared to be an important component of the overall selector-selectand interactions.

Overall, five types of noncovalent interactions can be rationalized in the formation of the 2:1 DCV-γ-CD complex as well as the plateau observed in CE (Krait et al., 2020) and the slow equilibration found in ITC:

(1) intramolecular HBs within DCV molecules stabilizing the folded conformation,
(2) intermolecular HBs between DCV and γ-CD and between 2 DCV molecules resulting in the formation of the DCV dimer,
(3) intramolecular and intermolecular interactions based on the electron charge density distribution of the solute,
(4) stacking π-π interactions between the biphenyl structures of DCV molecules, and
(5) steric (repulsive) interactions between the DCV dimer and γ-CD.

Considering the contributions of the processes discussed for rationalizing the plateau observed in CE, i.e., the slow dissociation of the 2:1 complex because of the folded conformation of the MOC-Val moieties versus the formation of a strong complex based on the complexation constant, it appears that the plateau in CE as a kinetic phenomenon might be primarily due to the slow dissociation. The high thermodynamic stability of the complex expressed as binding constant might also contribute resulting in a pronounced plateau even at low γ-CD concentrations.

3.2.2. Complex of DCV with TM-β-CD

The main structural differences between γ-CD and TM-β-CD refer to: (a) the size (8 and 7 α-D-glucopyranose units, respectively), (b) steric hindrance at both rims (due to the presence of the methyl groups in case of TM-β-CD) and (c) the shape of the CDs and consequently the shape of the CD cavities (Fig. S13, Supplementary material). As reported, the methylation at the 3-hydroxy groups of native β-CD impacts the distance between O_3n and O_2n, which increases from 2.9 to 3.5 Å (Steiner & Saenger, 1998). This weakens HB formation so that the round structure of native β-CD becomes elliptic. This trend was also confirmed for TM-β-CD by calculations (Fourtaka et al., 2018; Li et al., 2012) and X-ray diffraction analysis (Fourtaka et al., 2018; Halgren, 1999; Harata et al., 1983). In contrast, methylation of the 2-hydroxy groups of native β-CD does not affect the formation of O_3n···O_2n HBs, which form the interaction network resulting in the round structure observed in β-CD as well as the methylated derivatives 2-M-β-CD or 2,6-DM-β-CD (Harata, 1988; Steiner & Saenger, 1998). As a consequence, the crystal structures reported for TM-β-CD confirmed the distorted elliptical structure (Caira et al., 1994; Fourtaka et al., 2018; Harata et al., 1983; Harata et al., 1992; Shi et al., 2009; Steiner & Saenger, 1998). In particular, a structure with a fully inverted D-glucopyranose ring to the $^1C_4$ chair conformation was crystallized from hot water (Caira et al., 1994; Steiner & Saenger, 1998). A conformational change in TM-β-CD with one $^0S_2$-twist boat D-glucopyranose unit was also observed in the crystal structure of inclusion complexes with iodophenol and 4-biphenylacetic acid (Harata et al., 1992). Because DCV also contains a biphenyl moiety, the crystal structure of TM-β-CD with the distinctive $^0S_2$ conformation (CSD entry GELKEN10 (Harata et al., 1992)) was selected as starting structure to model this CD (Fig. S14, Supplementary material). The elliptic shape of the macrocycle was confirmed by the high value of $\Delta R_{l\text{-}s}$ = 2.133 Å determined as the calculated difference between the longest and the shortest O···O distances from the four pairs of opposing glycosidic O_gn-atoms ($1 \leq n \leq 7$) of TM-β-CD. Thus, compared to γ-CD, the cavity of TM-β-CD was substantially more elliptic, smaller and less accessible due to the steric hindrance exerted by the methyl groups at both rims. Consequently, the possibility of the formation of 2:1 complexes between DCV and TM-β-CD appeared to be rather unlikely if not impossible for obvious steric reasons. ITC data also confirmed the sole formation of a 1:1 complex between DCV and this CD.

As a consequence, only the 1:1 complexes between TM-β-CD and DCV as well as *RRRR*-DCV were explored by MD calculations. In accordance with the conditions used for the γ-CD complexes, MD simulations were performed over 100 ns in the AMBER force field by treating water as solvent explicitly. As shown in Fig. 7, the 1:1 complexes of TM-β-CD with DCV or *RRRR*-DCV displayed similar interaction energies. The mean interaction energy (approx. −80.9 kcal·mol^{-1}) (Table 4) was lower compared to the energies extracted for the 2:1 γ-CD complexes (102.9 and 103.5 kcal·mol^{-1} for DCV and RRRR-DCV, respectively). Moreover, the contribution of E_{vdW}, expressed as the percentage of the total interaction energy, was 45 %/46 % (Table 4). Thus, the entity of the percentual E_{vdW} contribution in both complexes, the 1:1 enantiomer-TM-β-CD and the 2:1 enantiomer-γ-CD complexes, was rather similar, being 41 %/46 % for the 2:1 enantiomer-γ-CD associates (Table 2).

In the representative snapshot of the most frequent DCV-TM-β-CD 1:1 complexes extracted over 100 ns of MD shown in Fig. 8, DCV appeared to be constrained inside the CD cavity by the methyl groups located at both rims. This steric effect may be considered as the likely cause of the plateau phenomenon observed in CE (Krait et al., 2021), assuming that the plateau represented the equilibrium between free and complexed analyte and that the steric constriction exerted by the methyl substituents of the CD considerably slowed the dissociation of the complex. It is worth to mention that the formation of inclusion complexes with reduced or blocked penetration of the analyte into the CD cavity were observed for TM-β-CD in the solid state as the effect of the hindrance exerted by the methyl groups (Harata, 1988). These act as a

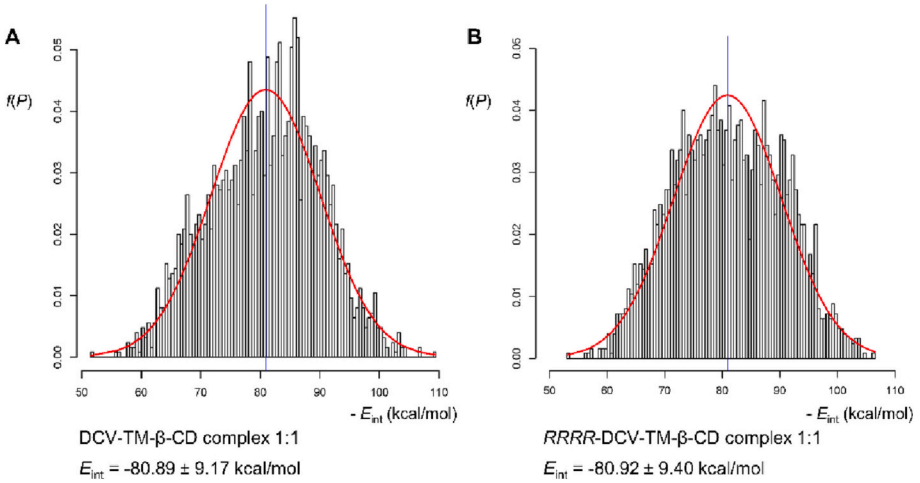

Fig. 7. Distribution of interaction energies of DCV-TM-β-CD (A) and *RRRR*-DCV-TM-β-CD (B) complexes (1:1) over 3 cycles of 100 ns MDs (2500 frames/simulation).

Table 4
Mean interaction energies of the DCV-TM-β-CD and *RRRR*-DCV-TM-β-CD complexes extracted by MD trajectories.

Molecular system	$E_{interaction}$ (kcal·mol^{-1})	E_{el} (kcal·mol^{-1})	E_{vdW} (kcal·mol^{-1})
DCV-TM-β-CD (1:1)	−80.89 ± 9.17	−44.62 ± 11.63	−36.27 ± 4.98
RRRR-DCV-TM-β-CD (1:1)	−80.92 ± 9.40	−43.45 ± 11.71	−37.27 ± 5.67

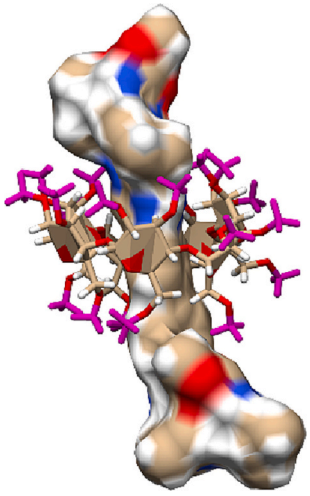

Fig. 8. Representative snapshot of the most frequent DCV-TM-β-CD 1:1 complexes observed over 100 ns of MD simulations. Color legend: blue, nitrogen; magenta, methyl; red, oxygen; tan, carbon; white, hydrogen. (For interpretation of the references to color in this figure legend, the reader is referred to the web version of this article.)

lid closing the narrower rim and making the CD cup-shaped (Caira et al., 1994). On the other hand, intra- and intermolecular HBs could be observed also for this complex. Three intramolecular HBs were found in the DCV molecule with a lifetime of 23, 8, and 3 ns, respectively, over 100 ns MD simulation. Moreover, two intermolecular HBs were detected involving the N—H of DCV as donor and the glucosyl oxygens of the CD as acceptor with a lifetime of 21 and 20 ns, respectively.

The contribution of the high-energy water from the cavity of CD was also quantified for TM-β-CD in terms of the number of water molecules liberated from the cavity upon inclusion of the analyte. However, the low values derived from MD trajectories (Table S5) revealed only a negligible effect compared to that observed for the complex formation in case of γ-CD. On the other hand, the pivotal role of water in determining the CE observations was highlighted by a comparison of both MMFF94 and PM6 semiempirical $\Delta E_{binding}$ calculated in vacuum and in water (implicitly the SM5.4 solvation model) for the 1:1 complexes between TM-β-CD and DCV or *RRRR*-DCV (Table 5). It was confirmed that neglecting the role of water provided $\Delta E_{binding} = -4.99$ kcal·mol^{-1} (MMFF94) versus −9.01 kcal·mol^{-1} (PM6). Introducing implicitly the parametrization of water, $\Delta E_{binding}$ close to zero was obtained with both MMFF94 and PM6 semiempirical. This is in agreement with the CE data, i.e. the lack the separation of DCV and its enantiomer when TM-β-CD was used as chiral selector (Krait et al., 2021) although this may also be an effect of the slow kinetics resulting in the plateau rather than a lack of enantiorecognition.

Table 5
Binding energies of the DCV-TM-β-CD and *RRRR*-DCV-TM-β-CD complexes calculated in vacuum and water (SM5.4 model) with the MMFF94s force field and PM6 semiempirical.

Medium	Enantiomer	Energy (kcal·mol^{-1})		
		MMFF94		PM6
		$E_{binding}$	$\Delta E_{binding}$[a]	$\Delta E_{binding}$[a]
Vacuum	DCV	−62.62	−4.99	−9.01
	RRRR	−57.63		
Water	DCV	−36.22	0.34	−0.64
	RRRR	−36.56		

[a] $\Delta E_{binding} = E_{binding\ (DCV)} - E_{binding\ (RRRR)}$.

4. Conclusions

In CE, two peaks with a plateau in between were observed when DCV was analyzed in an electrolyte containing γ-CD or TM-β-CD as well as the situation when the CDs were only present in combination with DCV in the sample, which was analyzed using CD-free buffer (Krait et al., 2020; Krait et al., 2021). Both observations indicated slow equilibria of the DCV-CD complexes. Attempting to rationalize these phenomena, ITC and theoretical calculations were performed. Both confirmed the presence of a 2:1 DCV-CD complex in case of γ-CD and a 1:1 complex in the presence of TM-β-CD, which had been concluded earlier from NMR and MS studies (Krait et al., 2020, Krait et al., 2021).

A model for the complexation of DCV is outlined in Fig. 9 for γ-CD (Fig. 9A) and TM-β-CD (Fig. 9B) considering different processes. In aqueous solution, there is an equilibrium between monomeric DCV and the DCV dimer (equilibrium 1). The dimer may be included into the

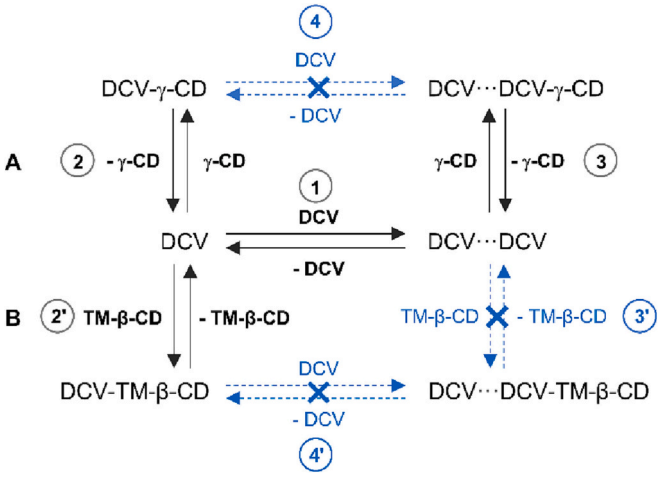

Fig. 9. Multi-step mechanisms profiled for 2:1 DCV-γ-CD (A) and 1:1 TM-β-CD (B) complex formation equilibria.

large cavity of γ-CD (equilibrium 3), where it is "fixed" due to restraints of the folded terminal MOC-Val moieties, which act as a clip toward the CD rims. The formation of a 1:1 DCV-γ-CD complex is possible (equilibrium 2) but the resulting complex is rather instable. Dissociation of one of the DCV molecules in the 2:1 complex (equilibrium 4) seems unlikely due to the fixation of the DCV dimer inside the γ-CD cavity so that this equilibrium is considered "forbidden". Overall, the process appears to be dominated by the slow dissociation of the 2:1 complex, although the high complexation constant could also contribute to the observed phenomena.

In case of TM-β-CD, access to the cavity is restricted by the methylation of the hydroxy groups on the narrower primary rim as well as the wider secondary rim. In combination with the smaller cavity size of this CD, the inclusion of the DCV dimer is impossible, so that equilibria 3′ as well as 4′ are not feasible, i.e., forbidden. TM-β-CD can only form a 1:1 complex with DCV (equilibrium 2′). Upon complexation, the solute is constrained by the methyl substituents on both rims exerting a clamp effect on the solute. Thus, it may be speculated that despite complex formation between DCV and TM-β-CD as well as the corresponding thermodynamic data are much lower compared to γ-CD, slow dissociation of the complex resulted in the plateau phenomenon observed in CE.

The initial hypothesis was, whether the cause for the plateau phenomenon observed in CE for both CDs has a common origin such as high stability of the complexes expressed as binding constants or may be based on different effects. Based on the present data it can be concluded that there is a common cause in case of both CDs, but this may rather be due to the slow dissociation of the complexes because of the steric hindrance exerted by the folded conformation of the MOC-Val moieties. In case of TM-β-CD additional steric constrains due to the methyl substituents exist. This results in overall slow dissociation although the complex is rather weak based on the low binding constant. In the case of γ-CD, the high stability of the complex might contribute to the overall stability and probably also slower complex dissociation, which also results in a more pronounced plateau in CE as compared to TM-β-CD. In this context one has to consider that the dynamics of the inclusion process of a solute into the CD cavity is a complex multistep process and rather challenging to deconvolute (Al-Soufi et al., 2008). It is reasonable to assume that the overall stability of CD inclusion complexes may be dictated by both association and dissociation processes between CDs and DCV. Likely, thermodynamics alone cannot explain the observed behavior in CE, which rather derives from a balance between thermodynamic and kinetic effects. In particular, as reported for CD complexes involving sterically hindered analytes, the dissociation constant may decrease due to the steric hindrance, impacting the overall stability of the complexes (Al-Soufi et al., 2005; Al-Soufi et al., 2008).

CRediT authorship contribution statement

Paola Peluso: Formal analysis, Writing – original draft, Writing – review & editing. **David Landy:** Formal analysis, Writing – review & editing. **Lamia Nakhle:** Data curation, Formal analysis. **Roberto Dallocchio:** Data curation, Formal analysis. **Alessandro Dessì:** Data curation, Formal analysis. **Sulaiman Krait:** Writing – review & editing. **Antonio Salgado:** Writing – review & editing. **Bezhan Chankvetadze:** Conceptualization, Writing – review & editing. **Gerhard K.E. Scriba:** Conceptualization, Supervision, Writing – review & editing.

Declaration of competing interest

The authors declare that they have no known competing financial interests or personal relationships that could have appeared to influence the work reported in this paper.

Data availability

Data will be made available on request.

Acknowledgements

The authors thank Mylan Laboratories Ltd. (Hyderabad, India) for a sample of DCV dihydrochloride.

Appendix A. Supplementary data

Supplementary data to this article can be found online at https://doi.org/10.1016/j.carbpol.2023.120870.

References

Al-Soufi, W., Reija, B., Felekyan, S., Seidel, C. A. M., & Novo, M. (2008). Dynamics of supramolecular association monitored by fluorescence correlation spectroscopy. *ChemPhysChem, 9*, 1819–1827. https://doi.org/10.1002/cphc.200800330

Al-Soufi, W., Reija, B., Novo, M., Felekyan, S., Kühnemuth, R., & Seidel, C. A. M. (2005). Fluorescence correlation spectroscopy, a tool to investigate supramolecular dynamics: Inclusion complexes of pyronines with cyclodextrin. *Journal of the American Chemical Society, 127*, 8775–8794. https://doi.org/10.1021/ja0508976

Basma, M., Sundara, S., Calgan, D., Venali, T., & Woods, R. J. (2001). Solvated ensemble averaging in the calculation of partial atomic charges. *Journal of Computational Chemistry, 22*, 1125–1137. https://doi.org/10.1002/jcc.1072

Bertaut, E., & Landy, D. (2014). Improving ITC studies of cyclodextrin inclusion compounds by global analysis of conventional and non-conventional experiments. *Beilstein Journal of Organic Chemistry, 10*, 2630–2641. https://doi.org/10.3762/bjoc.10.275

Bouchemal, K., & Mazzaferro, S. (2012). How to conduct and interpret ITC experiments accurately for cyclodextrin-guest interactions. *Drug Discovery Today, 17*, 623–629. https://doi.org/10.1016/j.drudis.2012.01.023

Caira, M. R., Griffith, V. J., Nassimbeni, L. R., & van Oudtshoorn, B. (1994). Unusual 1C4 conformation of a methylglucose residue in crystalline permethyl-β-cyclodextrin monohydrate. *Journal of the Chemical Society, Perkin Transactions, 2*, 2071–2072. https://doi.org/10.1039/P29940002071

Case, C. A., Ben-Shalom, I. Y., Brozell, S. R., Cerutti, D. S., Cheatham, T. E., III, Cruzeiro, V. W. D., … Kollman, P. A. (2018). *Amber 2018*. San Francisco: University of California.

Case, D. A., Cheatham, T. E., 3rd, Darden, T., Gohlke, H., Luo, R., Merz, K. M., Jr., Onufriev, A., Simmerling, C., Wang, B., & Woods, R. J. (2005). The AMBER biomolecular simulation programs. *Journal of Computational Chemistry, 26*, 1668–1688. https://doi.org/10.1002/jcc.20290

Catenacci, L., Sorrenti, M., Bonferoni, M. C., Hunt, L., & Caira, M. R. (2020). Inclusion of the phytoalexin trans-resveratrol in native cyclodextrins: A thermal, spectroscopic, and X-ray structural study. *Molecules, 25*, 998. https://doi.org/10.3390/molecules25040998

Chambers, C. C., Hawkins, G. D., Cramer, C. J., & Truhlar, D. G. (1996). Model for aqueous solvation based on class IV atomic charges and first solvation shell effects. *Journal of Physical Chemistry, 100*, 16385–16398. https://doi.org/10.1021/jp9610776

Chankvetadze, B. (2018). Contemporary theory of enantioseparations in capillary electrophoresis. *Journal of Chromatography A, 1567*, 2–25. https://doi.org/10.1016/j.chroma.2018.07.041

Core Team. (2017). *A language and environment for statistical computing*. Vienna, Austria: R Foundation for Statistical Computing. https://www.R-project.org.

Darden, T., York, D., & Pedersen, L. (1993). Particle mesh ewald: Anan N·log(N) method for ewald sums in large systems. *Journal of Chemical Physics, 98*, 10089–10092. https://doi.org/10.1063/1.464397

Elbashir, A. A. (2012). Combined approach using capillary electrophoresis and molecular modeling for an understanding of enantioselective recognition mechanisms. *Journal of Applied Solution Chemistry and Modeling, 1*, 121–126. https://doi.org/10.6000/1929-5030.2012.01.02.7

Elbashir, A. A., & Aboul-Enein, H. Y. (2013). Capillary electrophoresis and molecular modeling as a complementary technique for chiral recognition mechanism. *Critical Reviews in Analytical Chemistry, 43*, 131–137. https://doi.org/10.1080/10408347.2013.803358

Fanali, S., & Chankvetadze, B. (2019). Some thoughts about enantioseparations in capillary electrophoresis. *Electrophoresis, 40*, 2420–2437. https://doi.org/10.1002/elps.201900144

Fejös, I., Kalydi, E., Malanga, M., Benkovics, G., & Beni, S. (2020). Single isomer cyclodextrins as chiral selectors in capillary electrophoresis. *Journal of Chromatography A, 1627*, Article 461375. https://doi.org/10.1016/j.chroma.2020.461375

Fourtaka, K., Christoforides, E., Mentzafos, E., & Bethanis, K. (2018). Crystal structures and molecular dynamics studies of the inclusion compounds of β-citronellol in β-cyclodextrin, heptakis(2,6-di-O-methyl)-β-cyclodextrin and heptakis(2,3,6-tri-O-methyl)-β-cyclodextrin. *Journal of Molecular Structure, 1161*, 1–8. https://doi.org/10.1016/j.molstruc.2018.02.037

Guo, C., & Xiao, Y. (2021). Negatively charged cyclodextrins: Synthesis and applications in chiral analysis - A review. *Carbohydrate Polymers, 256*, Article 117517. https://doi.org/10.1016/j.carbpol.2020.117517

Halgren, T. A. (1999). MMFF VI. MMFF94s option for energy minimization studies. *Journal of Computational Chemistry, 20*, 720–729. https://doi.org/10.1002/(SICI)1096-987X(199905)20:7<720::AID-JCC7>3.0.CO;2-X

Hansen, L. D., Fellingham, G. W., & Russell, D. J. (2011). Simultaneous determination of equilibrium constants and enthalpy changes by titration colorimetry: Methods, instruments, and uncertainties. *Analytical Biochemistry, 409*, 220–229. https://doi.org/10.1016/j.ab.2010.11.002

Harata, K. (1988). The structure of the cyclodextrin complex. XXI. Crystal structures of heptakis(2,6-di-O-methyl)-β-cyclodextrin complexes with p-iodophenol and p-nitrophenol. *Bulletin of the Chemical Society of Japan, 61*, 1939–1944. https://doi.org/10.1246/bcsj.61.1939

Harata, K., Hirayama, F., Arima, H., Uekama, K., & Miyaji, T. (1992). Crystal structure of heptakis(2,3,6-tri-O-methyl)-β-cyclodextrin complexes with m-iodophenol and 4-biphenylacetic acid. Guest-induced conformational change of a pyranose ring. *Journal of the Chemical Society, Perkin Transactions, 2*, 1159–1166. https://doi.org/10.1039/P29920001159

Harata, K., Uekama, K., Otairi, M., & Hirayama, F. (1983). The structure of the cyclodextrin comple. XVI. Crystal structure of heptakis(2,3,6-tri-O-methyl)-β-cyclodextrin-p-iodophenol (1:1) complex tetrahydrate. *Bulletin of the Chemical Society of Japan, 56*, 1732–1736. https://doi.org/10.1246/bcsj.56.1732

Jakalian, A., Bush, B. L., Jack, D. B., & Bayly, I. (2000). Fast, efficient generation of high-quality atomic charges. AM1-BCC model: I. *Method. Journal of Computational Chemistry, 21*, 132–146. https://doi.org/10.1002/(SICI)1096-987X(20000130)21:2<132::AID-JCC5>3.0.CO;2-P

Kirschner, K. N., & Woods, R. J. (2001). Solvent interactions determine carbohydrate conformation. *Proceedings of the National Academy of Sciences (PNAS), 98*, 10541–10545. https://doi.org/10.1073/pnas.191362798

Kirschner, K. N., & Woods, R. J. (2001b). Quantum mechanical study of the nonbonded forces in water−methanol complexes. *Journal of Physical Chemistry A, 105*, 4150–4155. https://doi.org/10.1021/jp004413y

Krait, S., Salgado, A., Peluso, P., Malanga, M., Sohajda, T., Benkovics, G., Naumann, L., Neusüß, C., Chankvetadze, B., & Scriba, G. K. E. (2021). Complexation of daclatasvir by single isomer methylated β-cyclodextrins studied by capillary electrophoresis, NMR spectroscopy and mass spectrometry. *Carbohydrate Polymers, 273*, Article 118486. https://doi.org/10.1016/j.carbpol.2021.118486

Krait, S., Salgado, A., Villani, C., Naumann, L., Neusüß, C., Chankvetadze, B., & Scriba, G. K. E. (2020). Unusual complexation behavior between daclatasvir and γ-cyclodextrin. A multiplatform study. *Journal of Chromatography A, 1628*, Article 461448. https://doi.org/10.1016/j.chroma.2020.461448

Li, W.-S., Wang, S.-C., Hwang, T.-S., & Chao, I. (2012). Substituent effect on the structural behavior of modified cyclodextrin: A molecular dynamic study on methylated β-CDs. *Journal of Physical Chemistry B, 116*, 3477–3489. https://doi.org/10.1021/jp207985q

Pawlotsky, J.-M., Negro, F., Aghemo, A., Berenguer, M., Dalgard, O., Dusheiko, G., Marra, F., Puoti, M., & Wedemeyer, H. (2018). EASL recommendations on treatment of hepatitis C 2018. *Journal of Hepatology, 69*, 461–511. https://doi.org/10.1016/j.jhep.2018.03.026

Peluso, P., & Chankvetadze, B. (2021). Native and substituted cyclodextrins as chiral selectors for capillary electrophoresis enantioseparations: Structure, features, application, and molecular modeling. *Electrophoresis, 42*, 1676–1708. https://doi.org/10.1002/elps.202100053

Peluso, P., Dessi, A., Dallocchio, R., Mamane, V., & Cossu, S. (2019). Recent studies of docking and molecular dynamics simulation for liquid-phase enantioseparations. *Electrophoresis, 40*, 1881–1896. https://doi.org/10.1002/elps.201800493

Pettersen, E. F., Goddard, T. D., Huang, C. C., Couch, G. S., Greenblatt, D. M., Meng, E. C., & Ferrin, T. E. (2004). UCSF chimera - a visualization system for exploratory research and analysis. *Journal of Computational Chemistry, 25*, 1605–1612. https://doi.org/10.1002/jcc.20084

Rekharsky, M. V., & Inoue, Y. (1998). Complexation thermodynamics of cyclodextrins. *Chemical Reviews, 98*, 1875–1918. https://doi.org/10.1021/cr9700150

Roe, D. R., & Cheatham, T. E., 3rd (2013). PTRAJ and CPPTRAJ: Software for processing and analysis of molecular dynamics trajectory data. *Journal of Chemical Theory and Computation, 9*, 3084–3095. https://doi.org/10.1021/ct400341p

Salomon-Ferrer, R., Götz, A. W., Poole, D., Le Grand, S., & Walker, R. C. (2013). Routine microsecond molecular dynamics simulations with AMBER on GPUs. 2. Explicit solvent particle mesh Ewald. *Journal of Chemical Theory and Computation, 9*, 3878–3888. https://doi.org/10.1021/ct400314y

Sandilya, A., Natarajan, U., & Priya, M. H. (2020). Molecular view into the cyclodextrin cavity: Structure and hydration. *ACS Omega, 5*, 25655–25667. https://doi.org/10.1021/acsomega.0c02760

Saz, J. M., & Marina, M. L. (2016). Recent advances on the use of cyclodextrins in the chiral analysis of drugs by capillary electrophoresis. *Journal of Chromatography A, 1467*, 79–94. https://doi.org/10.1016/j.chroma.2016.08.029

Shao, A., Molnar, L. F., Jung, Y., Kussmann, J., Ochsenfeld, C., Brown, S. T., Gilbert, A. T. B., Slipchenko, L. V., Levchenko, S. V., O'Neil, D. P., Di Stasio, R. A., Jr., & Head-Gordon, M. (2006). Advances in methods and algorithms in a modern quantum chemistry program package. *Physical Chemistry Chemical Physics, 8*, 3172–3191. https://doi.org/10.1039/B517914A

Shi, J., Guo, D.-S., Ding, F., & Liu, Y. (2009). Unique regioselective binding of permethylated β-cyclodextrin with azobenzene derivatives. *European Journal of Organic Chemistry, 923–931*. https://doi.org/10.1002/ejoc.200800829

Steiner, T., & Saenger, W. (1998). Closure of the cavity in permethylated cyclodextrins through glucose inversion, flipping, and kinking. *Angewandte Chemie International Edition, 37*, 3404–3407. https://doi.org/10.1002/(SICI)1521-3773(19981231)37:24<3404::AID-ANIE3404>3.0.CO;2-G

Thomas, I. R., Bruno, I. J., Cole, J. C., Macrae, C. F., Pidcok, E., & Wood, P. A. (2010). WebCSD: The online portal to the Cambridge structural database. *Journal of Applied Crystallography, 43*, 362–366. https://doi.org/10.1107/S0021889810000452

Walker, R. C., Crowley, M. F., & Case, D. A. (2008). The implementation of a fast and accurate QM/MM potential method in AMBER. *Journal of Computational Chemistry, 29*, 1019–1031. https://doi.org/10.1002/jcc.20857

Yu, R. B., & Quirino, J. P. (2019). Chiral selectors in capillary electrophoresis: Trends during 2017–2018. *Molecules, 24*, 1135. https://doi.org/10.3390/molecules24061135

Zhu, Q., & Scriba, G. K. E. (2016). Advances in the use of cyclodextrins as chiral selectors in capillary electrokinetic chromatography: Fundamentals and applications. *Chromatographia, 79*, 1403–1435. https://doi.org/10.1007/s10337-016-3167-0